

# Single Particle Configurations of the Excited States of $^{203}\text{Po}$

S. Chatterjee, A. Ghosh,\* D. Arora,† S. Das, B. Mondal, S. Samanta, R. Raut,‡ and S. S. Ghugre  
*UGC-DAE Consortium for Scientific Research, Kolkata Centre, Kolkata 700098, India*

P. C. Srivastava

*Department of Physics, Indian Institute of Technology, Roorkee, Roorkee 247667, India*

A. K. Sinha§

*UGC-DAE Consortium for Scientific Research, University Campus, Khandwa Road, Indore 452017, India*

U. Garg

*Department of Physics, University of Notre Dame, Notre Dame, Indiana 46556*

H. K. Singh

*Department of Physics, Indian Institute of Technology, Bombay, Mumbai 400076, India*

Neelam and K. Rojeeta Devi

*Department of Physics and Astrophysics, University of Delhi, New Delhi 110007, India*

A. Sharma

*Department of Physics, Himachal Pradesh University, Shimla 171005, India*

S. S. Bhattacharjee, R. Garg, I. Bala, R. P. Singh, and S. Muralithar  
*Inter University Accelerator Centre, New Delhi 110067, India*

(Dated: July 5, 2022)

Excited states of the  $^{203}\text{Po}$  ( $Z = 84, N = 119$ ) have been investigated after populating them through  $^{194}\text{Pt}(^{13}\text{C},4n)$  fusion-evaporation reaction at  $E_{beam} = 74$  MeV and using a large array of Compton suppressed HPGe clover detectors as the detection setup for the emitted  $\gamma$ -rays. Standard techniques of  $\gamma$ -ray spectroscopy have been applied towards establishing the level structure of the nucleus. Twenty new  $\gamma$ -ray transitions have been identified therein, through  $\gamma - \gamma$  coincidence measurements, and spin-parity assignments of several states have been determined or confirmed, following the angular correlation and linear polarization measurements on the observed  $\gamma$ -rays. The excited states have been interpreted in the framework of large basis shell model calculations, while comparing their calculated and experimental energies. They have been principally ascribed to proton population in the  $h_{9/2}$  and  $i_{13/2}$  orbitals outside the  $Z = 82$  closure and neutron occupation of the  $f_{5/2}$ ,  $p_{3/2}$  and  $i_{13/2}$  orbitals in the  $N = 126$  shell.

PACS numbers: 23.20.Lv, 21.10.Hw, 21.60.Cs

## I. INTRODUCTION

The shell model of the nucleus has remained its most credible microscopic description through more than seven decades now. Testing the model across the nuclear chart and refining the inputs, towards accomplishing better overlap with data, has been an agenda of nuclear structure studies through their evolving practice. The exercise is facilitated by developments

in computational resources that help circumvent the dimensional challenges incurred in the application of shell model, particularly to heavier systems such as those around Pb ( $Z = 82$ ). It may be noted that the very validity of the shell model for describing level structures around the proton  $Z = 82$  closure was a subject of early investigations in the region. While the closure at  $Z = 82$  was identified to be sufficiently stable against collective excitations [1], it was also observed that light Hg ( $Z = 80$ ) isotopes do exhibit collectivity and there were predictions of similar phenomena in the proton-rich side of the ( $Z = 82$ ) closure, for the light Po ( $Z = 84$ ) nuclei [2]. The studies undertaken towards resolving the proposition, however, froze on describing the excitations of light-Po isotopes, such as  $^{199-201}\text{Po}$ , within the framework of the shell model. This was also commensurate with the systematically calculated [2] shapes of the Pb isotopes starting from  $^{208}\text{Pb}$  ( $Z = 82, N = 126$ ) and

\*Present Address: ONGC, Cinnamara Complex, Jorhat, Assam 785704, India

†Present Address: Inter University Accelerator Centre, New Delhi 110067, India

‡Corresponding Author: rajarshi.raut@gmail.com

§Presently: Hon. Adjunct Professor, Department of Physics, Savitribai Phule Pune University, Pune, India

extending to the lighter ones. The doubly-magic  $^{208}\text{Pb}$ , quite expectedly, exhibited deep energy minimum for a spherical shape; the minimum became shallower for lighter systems in the isotopic chain and eventually evolved into a double minima corresponding to both prolate and oblate deformations for nuclei as light as  $^{190}\text{Pb}$  ( $Z = 82, N = 108$ ). Such a scenario, however, wasn't established in  $^{198}\text{Pb}$  or  $^{202}\text{Pb}$  that still manifested near spherical shapes and it was found valid to interpret the excitation schemes of the neighboring light Po isotopes from the perspectives of the shell model. The merits of such interpretation notwithstanding, it was largely extracted from the evolution of experimentally observed level energies and their spacings across the isotopic and/or the isotonic chains. That was presumably owing to the limited wherewithal then available for computational endeavors but, nevertheless, could provide insights into the particle excitations underlying the level scheme of the nuclei being studied. The experimental findings in these studies mostly followed population of the nuclei of interest in  $\alpha$ - or heavy-ion induced fusion-evaporation reactions and detection of the  $\gamma$ -rays using modest setups of few Ge detectors and, at times, using conversion electron measurements alongwith.

The only existing precedence of spectroscopic study of the  $^{203}\text{Po}$  ( $Z = 84, N = 119$ ) nucleus, following its population in a fusion-evaporation reaction, was by Fant *et al.* [3]. The nucleus was populated using  $\alpha$ -induced reaction on  $^{204}\text{Pb}$  and the de-excitation  $\gamma$ -rays were detected using small planar Ge(Li) detectors, large coaxial Ge(Li) detectors and intrinsic Ge detectors. Conversion electrons were also measured in conjunction. The level scheme of the nucleus was established upto an excitation energy of  $\sim 4.4$  MeV and spin  $\sim 18\hbar$ . However, only a selected number of  $\gamma$ -ray transitions, presumably the strongest ones, and levels were identified above the  $25/2^+$  state; the spin-parity assignments were considerably tentative therein. The configurations of the excited states were largely ascribed to the coupling of an odd neutron hole to the excitations of the even  $^{204}\text{Po}$ -core ( $Z = 84, N = 120$ ). Two configurations, based on proton excitations outside the closed proton shell of the  $^{208}\text{Pb}$ -core, were identified in the latter. These were  $\pi h_{9/2}^2$  and  $\pi h_{9/2} i_{13/2}$  that resulted in maximum spins 8 and 11 respectively. The available single particle orbitals for the odd neutron are  $2f_{7/2}, 1h_{9/2}, 1i_{13/2}, 3p_{3/2}, 2f_{5/2}, 3p_{1/2}$  and the first  $5/2^-, 3/2^-, 1/2^-, 13/2^+$  states, in  $^{203}\text{Po}$ , were identified with single neutron excitations therein. The  $17/2^+, 21/2^+$ , and  $25/2^+$  yrast states in odd-A Po isotopes were attributed to the odd neutron hole  $\nu i_{13/2}^{-1}$  coupled to the excitations of the corresponding Pb-core or of the two valence protons of the Po-core, resulting in states  $2^+ - 8^+$ . This followed the systematics of the yrast states in odd-A Pb and Po isotones. It may be noted that the yrast  $17/2^+$  and the  $21/2^+$  states in isotones  $^{199-205}\text{Pb}$  had been ascribed to

pure neutron excitations, such as  $\nu p_{1/2}^{-1} f_{5/2}^{-1} i_{13/2}^{-1}$  and  $\nu f_{5/2}^{-2} i_{13/2}^{-1}$ . However, such (pure neutron) excitations would result into states of higher excitation energies than those of the yrast  $17/2^+$  and the  $21/2^+$  levels in odd-A Po isotopes. It was thus found reasonable to assign the pure neutron excitations to the respective non-yrast states. The  $27/2^+$  and the  $29/2^+$  levels in the odd Po nuclei were identified with three-quasiparticle configurations  $\pi h_{9/2}^2 \otimes \nu i_{13/2}^{-1}$ . The configurations for the isomeric  $25/2^-$  and  $29/2^-$  were derived from their overlap with the systematics of these states observed in the Pb isotopes. Accordingly, their configuration in  $^{203}\text{Po}$  was identified to be similar to that in  $^{201}\text{Pb}$  and the same is  $(\pi (h_{9/2}^2)_{0+} \otimes \nu p_{1/2}^{-2} f_{5/2}^{-3} (i_{13/2}^{-2})_{12+})_{25/2^- - 29/2^-}$ . The findings in  $^{203}\text{Po}$  thus upheld the interpretation of its excitation scheme within the framework of the single particle excitations, as had been established for the still lighter isotopes of the nucleus [2]. This was also a continuing trend from the heavier isotopes such as  $^{205,207}\text{Po}$  [1]. The absence of collectivity was further corroborated by the absence of enhanced B(E2) in these nuclei [3].

The present paper reports a spectroscopic investigation of the level structure of  $^{203}\text{Po}$ , using updated experimental facilities as well as contemporary framework for shell model calculations. The objective was to explore possible features in the excitation scheme of the nucleus, through the use of a large array of high-resolution gamma-ray detectors in the setup, and to test the reproducibility of the observed level energies in the calculations of the interacting shell model. The computational exercise is a validation of the model Hamiltonian used for the purpose as well as of facility in identifying and quantifying the single particle excitations that contribute to the observed level scheme.

## II. EXPERIMENTAL DETAILS AND DATA ANALYSIS

Excitations of the  $^{203}\text{Po}$  nucleus were investigated following its population in the  $^{194}\text{Pt}(^{13}\text{C}, 4n)$  reaction at  $E_{lab} = 74$  MeV. The target was 13 mg/cm<sup>2</sup> thick self-supporting foil of enriched (99%)  $^{194}\text{Pt}$ . The beam was delivered by the 15 UD Pelletron at IUAC, New Delhi and the beam energy was so chosen after an excitation function measurement at the commencement of the experiment. As per the predictions of the statistical model calculations, at this beam energy, the aforementioned reaction would be of dominant cross section amongst the possible compound nucleus fusion-evaporation channels while the fission (exit) channel would amount to  $\sim 25\%$  of the total fusion cross-section. Indeed, the yield of  $^{203}\text{Po}$  was observed to be maximum when compared to the other fusion-evaporation products that principally

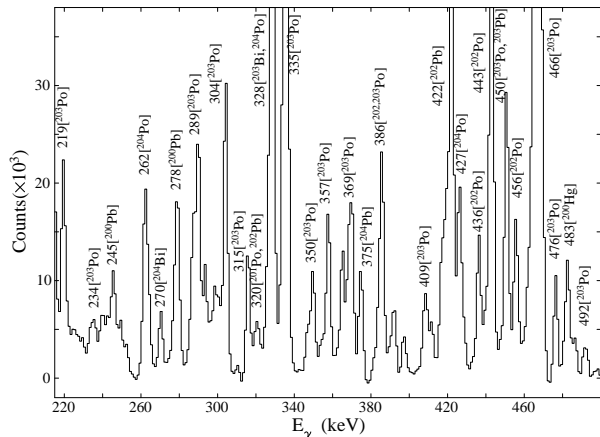


FIG. 1: Part of the  $\gamma$ -ray spectrum corresponding to the full projection of a  $\gamma$ - $\gamma$  symmetric matrix and illustrating the different product nuclei populated in the present experiment.

included isotopes of Po ( $Z = 84$ ), Bi ( $Z = 83$ ) and Pb ( $Z = 82$ ), as illustrated in Fig. 1. The detection system was the Indian National Gamma Array (INGA) setup at IUAC [4] and (then) consisted of eighteen Compton suppressed HPGe clover detectors positioned at  $148^\circ$  (4 detectors),  $123^\circ$  (4 detectors),  $90^\circ$  (6 detectors),  $57^\circ$  (2 detectors), and  $32^\circ$  (2 detectors). An assembly of three absorber sheets of lead, tin, and copper was affixed on the face of the heavy metal collimator of the Anti Compton Shield (ACS) in each detector. The absorbers facilitated in reducing the intensity of the X-rays, from the thick target, being incident on the detectors (and thus contributing in the event trigger). Data was principally acquired under the condition that at least two Compton suppressed HPGe clover detectors needed to fire in coincidence for generating the event trigger. The two- and higher-fold events acquired was  $\sim 2 \times 10^9$ .

The data was sorted into spectra, symmetric and asymmetric (angle dependent)  $\gamma$ - $\gamma$  matrices as well as  $\gamma$ - $\gamma$ - $\gamma$  cube using SPRINGZ [5] and INGASORT [6] codes and subsequently analyzed using the RADWARE [7] package. The methodology and the objectives of the exercise were identical to that of any regular investigation of nuclear level structure using  $\gamma$ -ray spectroscopy. These have been detailed in numerous papers, such as Ref. [8, 9], and are briefly mentioned herein. The coincidence relationships between the observed  $\gamma$ -ray transitions were extracted from the symmetric  $\gamma$ - $\gamma$  matrix and  $\gamma$ - $\gamma$ - $\gamma$  cube. The coincidences along with the intensity considerations were applied for the placement of the  $\gamma$ -ray transitions in the level scheme of the nucleus. The assignment of multiplicities of the  $\gamma$ -rays followed determination of their  $R_{ADO}$  (Ratio of Angular Distribution from Oriented Nuclei) values using

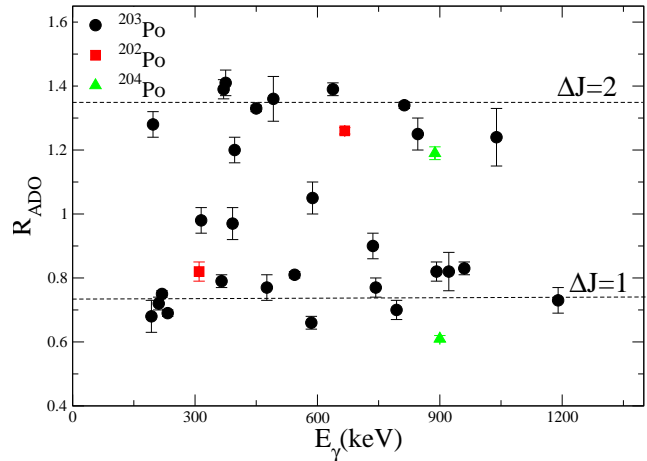


FIG. 2:  $R_{ADO}$  values for transitions of  $^{203}\text{Po}$ , as determined in the current analysis. Those for selected transitions of  $^{202,204}\text{Po}$  are plotted as reference.

$$R_{ADO} = \frac{I_{\gamma_1 \text{ at } 32^\circ \text{ (Gated by } \gamma_2 \text{ at all angles)}}}{I_{\gamma_1 \text{ at } 123^\circ \text{ (Gated by } \gamma_2 \text{ at all angles)}}} \quad (1)$$

where  $I$  is the intensity of the transition (of interest,  $\gamma_1$  in the above equation) in the relevant gated spectrum that is generated from the appropriate angle dependent matrix. As far as this analysis is concerned, the  $R_{ADO}$  value for the stretched dipole ( $\Delta J = 1$ ) transitions is  $0.73 \pm 0.01$  while for the stretched quadrupole ( $\Delta J = 2$ ) ones, it is  $1.34 \pm 0.01$ . These values were derived from  $R_{ADOS}$  of transitions with previously established multiplicities and belonging to other Po isotopes populated in the same experiment. The  $R_{ADO}$  values determined for different  $\gamma$ -ray transitions, observed in this study, are represented in Fig. 2.

The electromagnetic nature of the transitions were assigned on the basis of their polarization asymmetry evaluated using,

$$\Delta = \frac{aN_{\perp} - N_{\parallel}}{aN_{\perp} + N_{\parallel}} \quad (2)$$

where  $N_{\perp}$  and  $N_{\parallel}$  are respectively the number of photons of the  $\gamma$ -ray of interest that are scattered perpendicular to and parallel to the reference plane. The latter is defined by the beam direction and the direction of emission of the  $\gamma$ -ray. Each of the four crystals of a HPGe clover detector operates as scatterer while the two adjacent ones, parallel and perpendicular to the scatterer, operate as absorbers and facilitate in identifying the scattering events in the respective directions. The asymmetry between the two scattering possibilities is known to be maximum at  $90^\circ$ . Thus, the  $N_{\perp}$  ( $N_{\parallel}$ ) for  $\gamma$ -rays is extracted from a matrix

that has been constructed with the perpendicular (parallel) scattering events in the detectors at  $90^\circ$  on one axis and the coincident detections in detectors at all other angles on the other axis. The coincidences aid in the unambiguous identification of the  $\gamma$ -ray transition being analyzed. The  $a$  in Eq. (2) represents the asymmetry that is characteristic to the geometry of the detection setup. It was determined from the asymmetry between  $N_\perp$  and  $N_\parallel$  for  $\gamma$ -rays of (unpolarized) radioactive sources, such as  $^{152}\text{Eu}$ , and using  $a = N_\parallel/N_\perp$ . The typical plot of  $a$ , as a function of  $\gamma$ -ray energy, for the present setup is illustrated in Fig. 3(a). The observed asymmetry between  $N_\perp$  and  $N_\parallel$  for polarized  $\gamma$ -rays, such as those emitted by spin oriented ensemble of nuclei produced in fusion-evaporation reactions, depends on the degree of their polarization ( $P$ ) and the sensitivity ( $Q$ ) of the measurement setup. These are related through,

$$P = \frac{\Delta}{Q} \quad (3)$$

with,

$$Q(E_\gamma) = Q_0(E_\gamma)(CE_\gamma + D) \quad (4)$$

where,

$$Q_0(E_\gamma) = \frac{\alpha + 1}{\alpha^2 + \alpha + 1} \quad (5)$$

$\alpha$  being  $E_\gamma/m_e c^2$ ,  $m_e c^2$  is the electron rest mass energy. The  $C$  and  $D$  parameters for the purpose were adopted from those following the work by Palit *et al.* [10] and are  $C = 0.000099 \text{ keV}^{-1}$  and  $D = 0.446$ .

As per the regular methodology of nuclear structure studies, using  $\gamma$ -ray spectroscopy, the information on coincidence relationships between the  $\gamma$ -rays along with their intensities, multiplicities and electromagnetic nature, as resulting from the aforementioned analysis, were used to identify the excitation scheme of the nucleus and the same is discussed in the next section.

### III. RESULTS

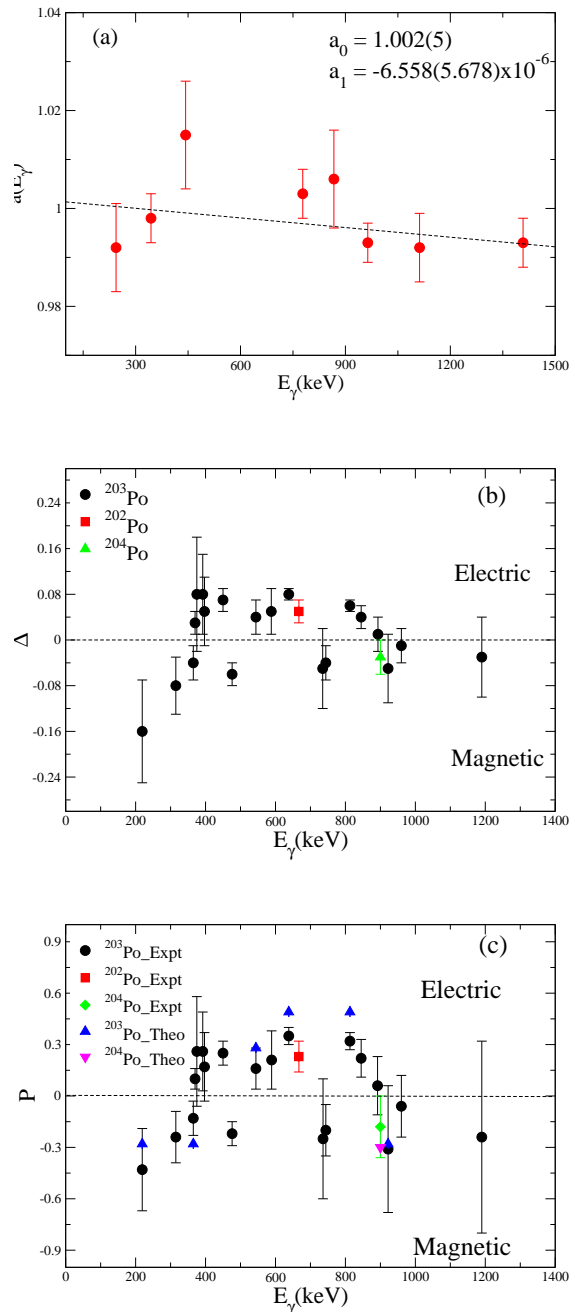


FIG. 3: (a) Plot of geometrical asymmetry as a function of  $\gamma$ -ray energy. (b) Polarization asymmetry of transitions of  $^{203}\text{Po}$ . (c) Linear polarization values for transitions of  $^{203}\text{Po}$  along with the corresponding theoretical estimates for some of them (of pure multipolarity). The  $\Delta$  and  $P$  values for selected transitions of other isotopes, that were populated in the same experiment, are included for validation.



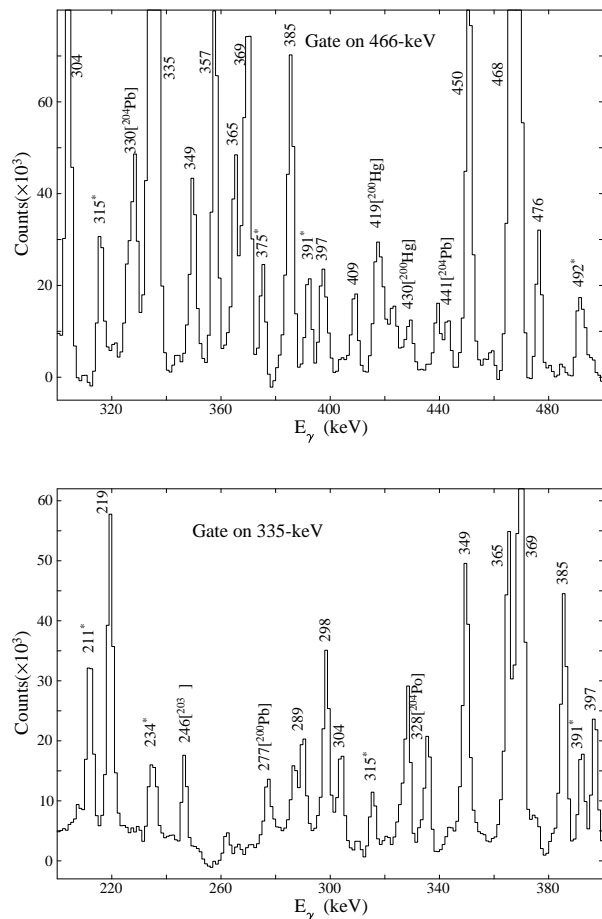


FIG. 5: Representative spectra projected out of  $\gamma\text{-}\gamma$  matrix with gate on transitions of  $^{203}\text{Po}$ , as indicated in the inset of the respective spectrum. The  $\gamma$ -rays newly identified in the present work are marked with \*. Those resulting from overlapping coincidences in other nuclei, populated in the same experiment, are also labeled accordingly.

The excitation scheme of  $^{203}\text{Po}$ , as established or confirmed in the present investigation, is illustrated in Fig. 4. Figs. 5 and 6 illustrate the representative gated spectra respectively projected from  $\gamma\text{-}\gamma$  matrix and  $\gamma\text{-}\gamma\text{-}\gamma$  cube. The observed coincidences have been used to identify the placement of transitions in the level scheme. Twenty new  $\gamma$ -ray transitions have been placed in the level scheme of the nucleus and the following modifications have been made in the existing [3, 11] assignments therein. The details of the  $\gamma$ -ray transitions are recorded in Table I. (The energies of the transitions and the levels are rounded off to the nearest integer in the discussions herein.)

1. The placement of 397-keV transition has been changed with respect to that assigned in the literature, as de-exciting a  $\sim 1527$ -keV level [12]. The level and the  $\gamma$ -ray was not reported by Fant *et al.* while in the present study the placement of the

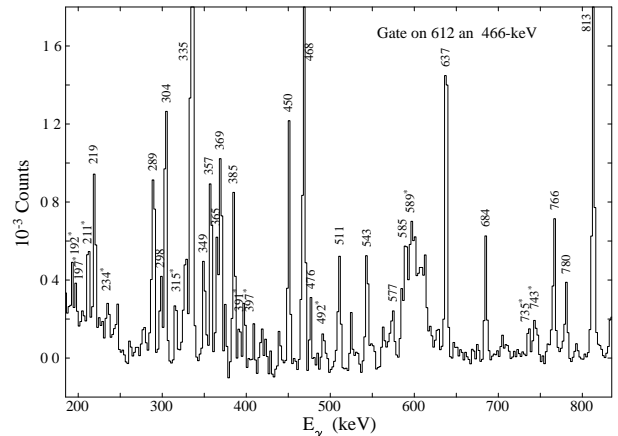


FIG. 6: Representative spectrum projected out of  $\gamma\text{-}\gamma\text{-}\gamma$  cube with double gate on transitions of  $^{203}\text{Po}$ , as indicated in the inset of the spectrum. The  $\gamma$ -rays newly identified in the present work are marked with \*.

transition has been modified to one de-exciting the  $\sim 3264$ -keV state. The level has been marked as a new one in the level scheme (Fig. 4) while the  $\gamma$ -ray transition is identified to have been observed previously, albeit with a different placement.

2. The 219-keV transition de-exciting the 2274-keV level has been identified as a M1 and the state has been identified to be of spin-parity  $27/2^+$ . There was no spin-parity assignment for this level, identified as  $\sim 2277$ -keV by Fant *et al.* [11], in the previous studies.
3. The 959-keV transition, de-exciting the 3014-keV state, has been assigned a mixed M1+(E2) nature, following the present measurements. Accordingly, the state has been assigned a spin-parity of  $27/2^+$  that is at variance with the assignment by Fant *et al.* [11]. The latter had identified the  $\gamma$ -ray as a pure E2 one and had tentatively assigned the spin-parity of the state ( $\sim 3018$ -keV, as per Fant *et al.*) as  $(29/2^+)$ .
4. The 543-keV  $\gamma$ -ray, from the 3066-keV state, has been assigned a multipolarity of E1 in this study. It was tentatively identified as M1, by Fant *et al.*, and the spin of the level (at  $\sim 3070$ -keV, as per Fant *et al.*) was accordingly assigned to be  $29/2$ .
5. The 585-keV transition de-exciting the 3108-keV state has been established as a pure dipole in this study. However, the electromagnetic nature of the same could not be unambiguously determined in the present investigation. The multipolarity of the transition was undetermined in the work by Fant *et al.* and consequently there was no spin assignment

for the state (at  $\sim 3112$ -keV, as quoted by Fant *et al.*) therein.

6. The spin-parity of the 3236-keV state, de-excited by the 369-keV transition, has been confirmed to be  $33/2^+$  in this study. The assignment for the level (at  $\sim 3241$ -keV, as per Fant *et al.*) was only tentative in the previous work [11].
7. The spin-parity of the 3712-keV level has been assigned as  $33/2^+$  in this work, following the E2 assignment of the 845-keV  $\gamma$ -ray that de-excites the state. There was no multipolarity assignment for the transition or spin-parity assignment for the state (at  $\sim 3717$ -keV, as per Fant *et al.*) in the previous studies [11].
8. The 3877-keV state has been assigned spin-parity of  $33/2^-$ , in this measurement. This is following the identification of the 450-keV transition, that de-excites the level, as an E2 one herein. Previously [11], the transition was assigned as M1 and the spin-parity of the state (at  $\sim 3882$ -keV, as quoted by Fant *et al.*) as  $31/2^-$ . Fig. 7 represents the spectra of the transition corresponding to the perpendicular and the parallel scattering events and illustrates the dominance of the former that leads to positive value of polarization asymmetry (Eq. 2) or polarization (Eq. 3).
9. The spin-parity of the 4352-keV level has been confirmed to be  $35/2^-$  in the present work. The assignment was tentative for the state (at  $\sim 4358$ -keV, quoted by Fant *et al.*) in the previous studies. The 476-keV transition, de-exciting the state, has been identified as M1 in this study and this is different from the E2 assignment by Fant *et al.*

An additional proposition can be put forth on the multipolarity assignment of the 182-keV transition de-exciting the 2156-keV state. Since the state is known to be an isomer of  $T_{1/2} > 200$  ns [3], the multipolarity of the transition could not be ascertained from its *ADO* ratio and its polarization asymmetry. These measurements are valid for transitions emitted by spin oriented ensemble of nuclei, such as produced in fusion-evaporation reactions, while the aforementioned isomeric lifetime is sufficient to induce dealignment. If the observed intensity of this 182-keV transition is corrected for electron conversion, using codes such as BrICC [13], it is  $\sim 60\%$  increased if the transition is an E2 one and  $\sim 300\%$  enhanced if it is a M1. The latter would result in an unbalanced intensity across the 1975-keV state that is fed by the 182-keV transition and de-excited by the 596-keV one. If the 182-keV transition is thus interpreted to be of E2 nature, the 2156-keV level can be assigned a spin-parity of  $25/2^+$ . However, since there is no direct experimental evidence for the same, this proposition has not been indicated in the level scheme (Fig. 4) and the assignment has

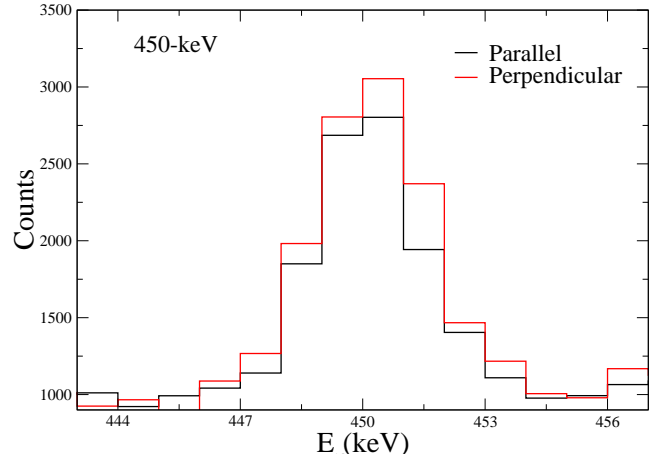


FIG. 7: Spectra of 450-keV transition peak corresponding to the perpendicular and the parallel scattering events in the HPGe clover detectors at  $90^\circ$ .

not been included in the table (Table I). The sharp decrease in the relative intensity of the  $\gamma$ -ray transitions across the 2156-keV state is also noteworthy and can be ascribed to the state being an isomer of  $T_{1/2} > 200$  ns [3].

Previous studies [3, 14] on the Po isotopes had reported a number of isomers therein. Some of these, with half-lives around few ns, have been reexamined in the current study using the centroid shift method [15, 16]. In the present implementation of the technique, the time difference between the feeding and the decaying  $\gamma$ -ray transitions of a state is histogrammed alternately by defining one as the start (stop) and the other as stop (start). The difference between the centroids of the two distribution is known to be  $2\tau$ ,  $\tau$  being the average lifetime of the state. Fig. 8 illustrates the time difference spectra between the (i) 788- and 262-keV transitions that respectively feeds and de-excites the 3387-keV state in  $^{204}\text{Po}$  [14], also populated in the present experiment, and (ii) 637- and 304-keV transitions that respectively feeds and de-excites the 2789-keV state in  $^{203}\text{Po}$ . The half-life of the 3387-keV state in  $^{204}\text{Po}$  was determined by Fant *et al.* [14] as  $9 \pm 3$  ns, presumably following an analysis of the time profile of the decaying transition with respect to the RF of the accelerator. The present analysis has resulted in  $T_{1/2} = 6.2 \pm 0.8$  ns, that is within the limits of uncertainty on the previous estimate and validates the present analysis. The latter carried out for the 2789-keV state in  $^{203}\text{Po}$  yields its  $T_{1/2} = 7.1 \pm 0.1$  ns that is lesser than the previous value, also reported by Fant *et al.* [3], of  $12 \pm 2$  ns.

The experimentally observed level scheme of the  $^{203}\text{Po}$  nucleus has been interpreted through single particle excitations in the framework of the shell model. The same is detailed in the next section.

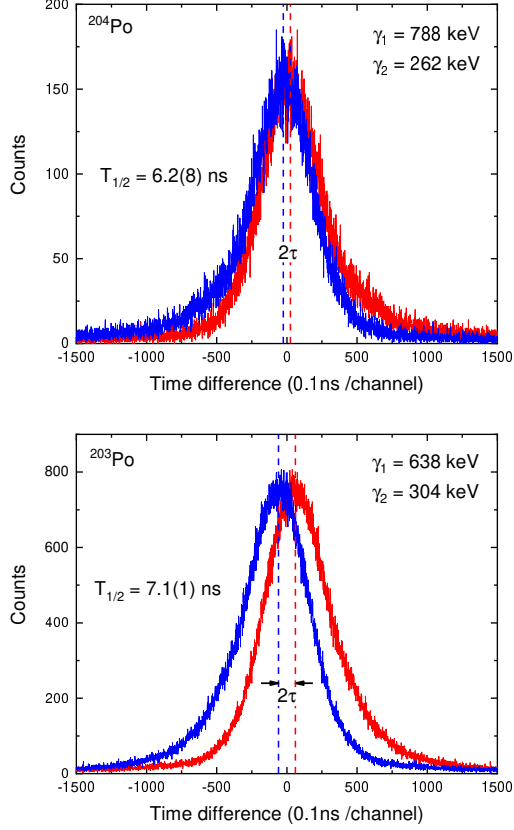


FIG. 8: (Color online) Time difference spectra between transitions indicated in the inset, for determining isomeric lifetimes. The upper panel corresponds to the state at 3387-keV state in  $^{204}\text{Po}$  while the bottom panel is for 2789-keV state in  $^{203}\text{Po}$ . (Please refer to the text for details.)

TABLE I: Details of the levels and the  $\gamma$ -ray transitions of  $^{203}\text{Po}$  nucleus observed in the present work. The energy of a  $\gamma$ -ray transition is the weighted average of its value in multiple gates. The relative intensities ( $I_\gamma$ ) of the  $\gamma$ -ray transitions are normalized with respect to the intensity of 466-keV transition as observed in 612-keV gated spectrum. The ADO ratios ( $R_{ADO}$ ), polarization asymmetry ( $\Delta_{pol}$ ), and linear polarization ( $P$ ) of the transitions are determined using the procedure described in Section II. The  $N$  and  $a$  superscripts indicate the assignments that have been respectively adopted from NNDC [11] and/or Fant *et al.* [3].

$E_i(\text{keV})$	$E_\gamma(\text{keV})$	$I_\gamma$	$J_i^\pi$	$J_f^\pi$	$R_{ADO}$	$\Delta_{pol}$	$P$	Multipolarity
$638.7 \pm 0.1$	$577.2 \pm 0.1$	$11 \pm 1$	$7/2^-$	$(3/2^-)$				$E2^N$
	$638.7 \pm 0.1$	$48 \pm 1$	$7/2^-$	$5/2^-$				$M1^N$
$641.7 \pm 0.2$	$641.7 \pm 0.2$		$13/2^+$	$5/2^-$				$M4^N$
$1055.2 \pm 0.1$	$416.5 \pm 0.1$	$59 \pm 1$	$(11/2^-)^a$	$7/2^-$				$M1+E2^N$
$1254.0 \pm 0.2$	$612.3 \pm 0.1$		$17/2^+$	$13/2^+$				$E2^N$
$1378.8 \pm 0.3$	$737.1 \pm 0.2$	$127 \pm 3$	$(17/2^+)^a$	$13/2^+$				$(E2)^N$
$1697.1 \pm 0.8$	$318.3 \pm 0.7$	$23 \pm 6$		$(17/2^+)^a$				
$1719.8 \pm 0.2$	$465.8 \pm 0.1$	1000	$21/2^+$	$17/2^+$				$E2^N$
$1974.5 \pm 0.3$	$595.7 \pm 0.1$	$251 \pm 2$	$(21/2^+)^a$	$(17/2^+)$				$E2^N$
$2054.7 \pm 0.2$	$334.9 \pm 0.1$	$643 \pm 14$	$25/2^+$	$21/2^+$				$E2^N$
$2077.0 \pm 0.2$	$356.8 \pm 0.1$	$64 \pm 2$	$21/2^+$	$21/2^+$				$M1^N$
$2156.4 \pm 0.3$	$181.9 \pm 0.1$	$156 \pm 1$		$(21/2^+)^a$				
$2184.4 \pm 0.7$	$805.6 \pm 0.6$	$4 \pm 1$		$(17/2^+)^a$				
$2273.6 \pm 0.2$	$219.1 \pm 0.1$	$58 \pm 1$	$27/2^+$	$25/2^+$	$0.75 \pm 0.01$	$-0.16 \pm 0.09$	$-0.43 \pm 0.24$	$M1$
$2404.2 \pm 0.2$	$349.2 \pm 0.1$	$36 \pm 1$	$25/2^+$	$25/2^+$				$M1^N$
	$684.1 \pm 0.1$	$71 \pm 2$	$25/2^+$	$21/2^+$				

Continued in next page



TABLE I – continued from previous page

$E_i(keV)$	$E_\gamma(keV)$	$I_\gamma$	$J_i^\pi$	$J_f^\pi$	$R_{ADO}$	$\Delta_{pol}$	P	Multipolarity
2485.8 ± 0.2	408.6 ± 0.2	21 ± 1	23/2 <sup>+</sup>	21/2 <sup>+</sup>				M1 <sup>N</sup>
	765.9 ± 0.1	76 ± 2	23/2 <sup>+</sup>	21/2 <sup>+</sup>				M1 <sup>N</sup>
2500.2 ± 0.2	780.1 ± 0.1	40 ± 1	23/2 <sup>+</sup>	21/2 <sup>+</sup>				(M1) <sup>N</sup>
2523.0 ± 0.2	468.3 ± 0.1	176 ± 4	27/2 <sup>+</sup>	25/2 <sup>+</sup>				M1 <sup>N</sup>
2527.6 ± 0.7	1148.8 ± 0.6			(17/2 <sup>+</sup> ) <sup>a</sup>				
2765.1 ± 0.4	710.4 ± 0.3	8 ± 1		25/2 <sup>+</sup>				
2789.1 ± 0.2	289.3 ± 0.1	74 ± 2	25/2 <sup>-</sup>	23/2 <sup>+</sup>				(E1) <sup>N</sup>
	303.5 ± 0.1	102 ± 2	25/2 <sup>-</sup>	23/2 <sup>+</sup>				E1 <sup>N</sup>
	385.1 ± 0.1	54 ± 2	25/2 <sup>-</sup>	25/2 <sup>+</sup>				E1 <sup>N</sup>
2820.9 ± 0.2	297.7 ± 0.1	28 ± 1	29/2 <sup>-</sup>	27/2 <sup>+</sup>				(E1) <sup>N</sup>
2863.0 ± 0.2	589.4 ± 0.1	55 ± 2	31/2 <sup>+</sup>	27/2 <sup>+</sup>	1.05 ± 0.05	0.05 ± 0.04	0.21 ± 0.17	E2+M3
2867.2 ± 0.2	812.5 ± 0.1	226 ± 5	29/2 <sup>+</sup>	25/2 <sup>+</sup>	1.34 ± 0.01	0.06 ± 0.01	0.32 ± 0.05	E2
2950.0 ± 0.4	793.6 ± 0.2				0.70 ± 0.03			D
2976.7 ± 0.3	922.2 ± 0.2	13 ± 1	27/2 <sup>+</sup>	25/2 <sup>+</sup>	0.82 ± 0.06	-0.05 ± 0.06	-0.31 ± 0.37	M1
3013.5 ± 0.2	959.1 ± 0.1	44 ± 1	27/2 <sup>+</sup>	25/2 <sup>+</sup>	0.83 ± 0.02	-0.01 ± 0.03	-0.06 ± 0.19	M1+(E2)
3066.1 ± 0.2	542.7 ± 0.1	46 ± 1	29/2 <sup>-</sup>	27/2 <sup>+</sup>	0.81 ± 0.01	0.04 ± 0.03	0.16 ± 0.12	E1
3093.2 ± 0.4	1038.5 ± 0.3	16 ± 3	29/2	25/2 <sup>+</sup>	1.24 ± 0.09			Q
3107.5 ± 0.2	584.5 ± 0.1	21 ± 1	29/2	27/2 <sup>+</sup>	0.66 ± 0.02			D
3108.3 ± 0.4	704.1 ± 0.3	11 ± 1		25/2 <sup>+</sup>				
3220.5 ± 0.4	1165.8 ± 0.3	6 ± 1		25/2 <sup>+</sup>				
3231.8 ± 0.2	364.5 ± 0.1	40 ± 1	31/2 <sup>+</sup>	29/2 <sup>+</sup>	0.79 ± 0.02	-0.04 ± 0.03	-0.13 ± 0.10	M1
3236.3 ± 0.2	368.8 ± 0.1	79 ± 2	33/2 <sup>+</sup>	29/2 <sup>+</sup>	1.39 ± 0.03	0.03 ± 0.02	0.10 ± 0.06	E2
3241.9 ± 0.2	374.7 ± 0.1	15 ± 1	33/2 <sup>+</sup>	29/2 <sup>+</sup>	1.41 ± 0.04	0.08 ± 0.10	0.26 ± 0.32	(E2)
3254.4 ± 0.2	390.9 ± 0.1	18 ± 1	33/2 <sup>-</sup>	31/2 <sup>+</sup>	0.97 ± 0.05	0.08 ± 0.07	0.26 ± 0.23	E1+M2
3262.9 ± 0.2	196.6 ± 0.1	16 ± 1	33/2	29/2 <sup>-</sup>	1.28 ± 0.04			Q
3264.0 ± 0.2	397.0 ± 0.1	22 ± 1	33/2 <sup>+</sup>	29/2 <sup>+</sup>	1.20 ± 0.04	0.05 ± 0.06	0.17 ± 0.20	(E2)
3292.0 ± 0.3	1237.2 ± 0.2	5 ± 1		25/2 <sup>+</sup>				
3416.1 ± 0.3	627.4 ± 0.2	17 ± 1		25/2 <sup>-</sup>				
3426.5 ± 0.2	637.3 ± 0.1	140 ± 3	29/2 <sup>-</sup>	25/2 <sup>-</sup>	1.39 ± 0.02	0.08 ± 0.01	0.35 ± 0.05	E2
3443.2 ± 0.3	211.4 ± 0.2	29 ± 1	33/2	31/2 <sup>+</sup>	0.72 ± 0.02			D
3456.2 ± 0.2	192.3 ± 0.1	11 ± 1	35/2	33/2 <sup>+</sup>	0.68 ± 0.05			D
3488.8 ± 0.3	234.3 ± 0.2	15 ± 1	35/2	33/2 <sup>-</sup>	0.69 ± 0.01			D
3603.8 ± 0.3	1329.9 ± 0.2	9 ± 1		27/2 <sup>+</sup>				
3711.9 ± 0.2	844.7 ± 0.1	29 ± 1	33/2 <sup>+</sup>	29/2 <sup>+</sup>	1.25 ± 0.05	0.04 ± 0.02	0.22 ± 0.11	E2
3741.7 ± 0.2	315.1 ± 0.1	34 ± 1	31/2 <sup>-</sup>	29/2 <sup>-</sup>	0.98 ± 0.04	-0.08 ± 0.05	-0.24 ± 0.15	M1+E2
3876.6 ± 0.2	450.3 ± 0.1	97 ± 2	33/2 <sup>-</sup>	29/2 <sup>-</sup>	1.33 ± 0.01	0.07 ± 0.02	0.25 ± 0.07	E2
3934.7 ± 0.3	491.5 ± 0.2	21 ± 1	37/2	33/2	1.36 ± 0.07			Q
3979.4 ± 0.3	742.9 ± 0.2	23 ± 1	35/2 <sup>+</sup>	33/2 <sup>+</sup>	0.77 ± 0.03	-0.04 ± 0.03	-0.20 ± 0.15	M1
4146.2 ± 0.2	891.8 ± 0.1	24 ± 1	35/2 <sup>+</sup>	33/2 <sup>-</sup>	0.82 ± 0.03	0.01 ± 0.03	0.06 ± 0.18	(E1)
4352.3 ± 0.2	475.9 ± 0.1	27 ± 1	35/2 <sup>-</sup>	33/2 <sup>-</sup>	0.77 ± 0.04	-0.06 ± 0.02	-0.22 ± 0.07	M1
4528.2 ± 0.4	175.9 ± 0.3	13 ± 1		35/2 <sup>-</sup>				
4612.0 ± 0.3	735.4 ± 0.2	26 ± 1	35/2 <sup>-</sup>	33/2 <sup>-</sup>	0.90 ± 0.04	-0.05 ± 0.07	-0.25 ± 0.35	M1+E2
4623.3 ± 0.4	746.7 ± 0.3	8 ± 1		33/2 <sup>-</sup>				
4645.6 ± 0.2	1189.3 ± 0.1	24 ± 1	37/2	35/2	0.73 ± 0.04	-0.03 ± 0.07	-0.24 ± 0.56	(M1)
4929.8 ± 0.5	1053.2 ± 0.4			33/2 <sup>-</sup>				

#### IV. DISCUSSIONS

One of the objectives of this endeavor has been to probe the efficacy of the shell model in interpreting the excitation scheme of the nuclei in the  $A \sim 200$  region. There have been similar efforts, in recent times, wherein level structures of nuclei around the  $^{208}\text{Pb}$ -core are calculated in the shell model framework. Bothe *et al.* [17] have reported such calculations for the isomeric states in  $^{203}\text{Tl}$  ( $Z = 81, N = 122$ ) while Yadav *et al.* [16] and Madhu *et al.* [15] have used them for deciphering

the particle excitations associated with the observed states of  $^{215,216}\text{Fr}$  ( $Z = 87, N = 128, 129$ ) nuclei. These studies have identified a general overlap, between the experimental and the calculated level energies, of within  $\sim 250$ -keV as reasonable.

Large basis shell model calculation has been carried out in the present work using KHH7B [18] Hamiltonian in the model space spanning  $Z = 58 - 114$  and  $N = 100 - 164$ . The latter includes proton orbitals  $d_{5/2}$ ,  $h_{9/2}$ ,  $d_{3/2}$  and  $s_{1/2}$  below  $Z = 82$  and the  $h_{9/2}$ ,  $f_{7/2}$

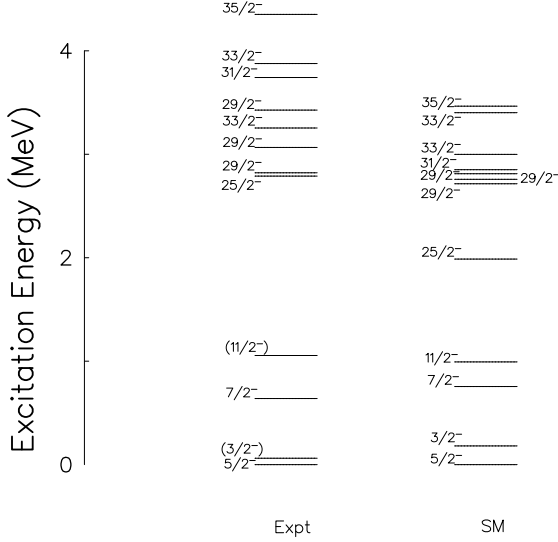


FIG. 9: Comparison between the calculated and the experimental level energies of the negative parity states in  $^{203}\text{Po}$ .

and  $i_{13/2}$  above; the neutron orbitals are  $i_{13/2}$ ,  $p_{3/2}$ ,  $f_{5/2}$ , and  $p_{1/2}$  below  $N = 126$  and the  $g_{9/2}$ ,  $i_{11/2}$ , and  $j_{15/2}$  above. Proton excitations across  $Z = 82$  closure and neutron excitations across the closure at  $N = 126$  have not been allowed in the calculations. The matrix diagonalization has been carried out using the OXBASH

[19] code. The comparison between the calculated and the experimental level energies is illustrated in Figs. 9 and 10. The dominant particle configurations along with the energy values of the states are recorded in Table II.

The calculated energies of the negative parity states with spin  $< 29/2$  are excellent overlap with their experimental values, even within  $\sim 100$ -keV for some of them. The  $25/2^-$  level is an exception for which the theoretical and the measured level energies differ by  $\sim 800$  keV. The dominant particle configurations associated with these states negative parity states have been calculated to be  $\pi(h_{9/2}^2) \otimes \nu(f_{5/2}^{3,2} p_{3/2}^{2,3} i_{13/2}^{14})$ . The negative parity states at higher spins,  $\geq 31/2$ , are poorly represented in the calculations wherein their energies are deviant by as much as 500-keV - 1-MeV with respect to the experimental values. The energy of the calculated yrast  $33/2^-$  state, however, reasonably overlaps with the measured energy within  $\sim 250$ -keV. The most probable particle configurations for the negative parity states at higher spins correspond to  $\pi(h_{9/2}^1 i_{13/2}^1) \otimes \nu(f_{5/2}^2 p_{3/2}^4 i_{13/2}^{13})$ . However, those of the yrare  $33/2^-$  and the  $35/2^-$  are different ( $\pi(h_{9/2}^2) \otimes \nu(f_{5/2}^3 p_{3/2}^4 i_{13/2}^{12})$ ) but, as indicated by the widely deviant calculated energies vis-a-vis the experimental ones, these configurations do not appropriately represent the relevant states, similar to the other high spin levels of odd parity.

TABLE II: Main partitions of wave functions of the positive and negative parity states in  $^{203}\text{Po}$  for KHH7B interaction

Level Energy		$J^\pi$	Probability	Proton	Neutron
EXPT	SM				
NEGATIVE PARITY					
0	0	$5/2^-$	29.33	$h_{9/2}^2 f_{7/2}^0 i_{13/2}^0$	$f_{5/2}^3 p_{3/2}^2 p_{1/2}^0 i_{13/2}^{14}$
62	181	$(3/2^-)$	39.21	$h_{9/2}^2 f_{7/2}^0 i_{13/2}^0$	$f_{5/2}^2 p_{3/2}^3 p_{1/2}^0 i_{13/2}^{14}$
639	755	$7/2^-$	19.96	$h_{9/2}^2 f_{7/2}^0 i_{13/2}^0$	$f_{5/2}^2 p_{3/2}^3 p_{1/2}^0 i_{13/2}^{14}$
1055	993	$(11/2^-)$	37.64	$h_{9/2}^2 f_{7/2}^0 i_{13/2}^0$	$f_{5/2}^2 p_{3/2}^3 p_{1/2}^0 i_{13/2}^{14}$
2789	1987	$25/2^-$	39.78	$h_{9/2}^2 f_{7/2}^0 i_{13/2}^0$	$f_{5/2}^3 p_{3/2}^2 p_{1/2}^0 i_{13/2}^{14}$
2821	2715	$29/2^-$	70.95	$h_{9/2}^2 f_{7/2}^0 i_{13/2}^0$	$f_{5/2}^3 p_{3/2}^2 p_{1/2}^0 i_{13/2}^{14}$
3066	2758	$29/2^-$	31.65	$h_{9/2}^2 f_{7/2}^0 i_{13/2}^0$	$f_{5/2}^3 p_{3/2}^4 p_{1/2}^0 i_{13/2}^{12}$
3254	2999	$33/2^-$	26.06	$h_{9/2}^1 f_{7/2}^0 i_{13/2}^1$	$f_{5/2}^2 p_{3/2}^4 p_{1/2}^0 i_{13/2}^{13}$
3427	2812	$29/2^-$	24.93	$h_{9/2}^1 f_{7/2}^0 i_{13/2}^1$	$f_{5/2}^2 p_{3/2}^4 p_{1/2}^0 i_{13/2}^{13}$
3742	2851	$31/2^-$	25.53	$h_{9/2}^1 f_{7/2}^0 i_{13/2}^1$	$f_{5/2}^2 p_{3/2}^4 p_{1/2}^0 i_{13/2}^{13}$
3877	3402	$33/2^-$	42.34	$h_{9/2}^2 f_{7/2}^0 i_{13/2}^0$	$f_{5/2}^3 p_{3/2}^4 p_{1/2}^0 i_{13/2}^{12}$

Continued in next page

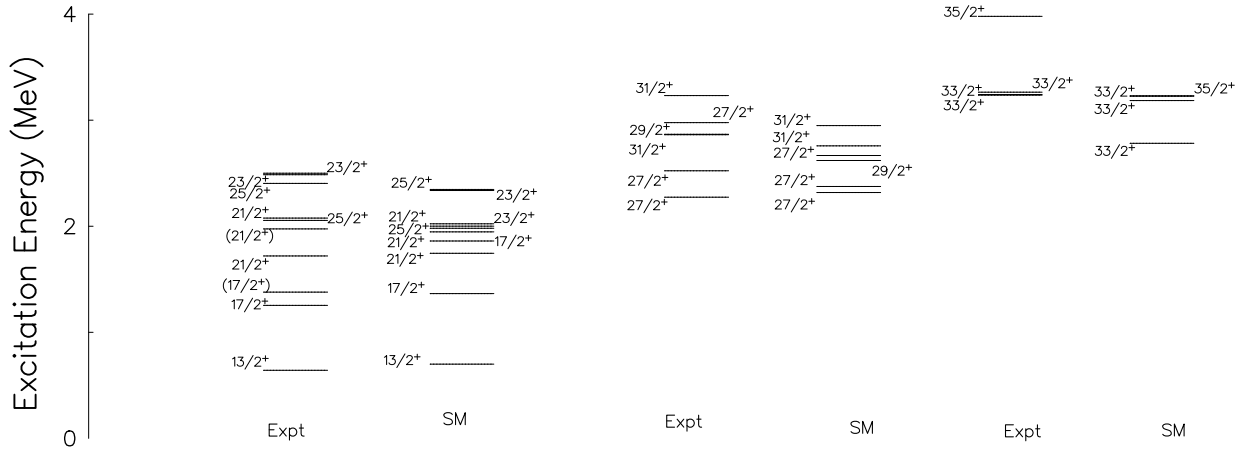


FIG. 10: Comparison between the calculated and the experimental level energies of the positive parity states in  $^{203}\text{Po}$ .

TABLE II – continued from previous page					
Level	Energy	$J^\pi$	Probability	Proton	Neutron
EXPT	SM				
4352	3465	$35/2^-$	24.51	$h_{9/2}^1 f_{7/2}^0 i_{13/2}^1$	$f_{5/2}^2 p_{3/2}^4 p_{1/2}^0 i_{13/2}^1$
4612	3671	$35/2^-$	29.32	$h_{9/2}^2 f_{7/2}^0 i_{13/2}^0$	$f_{5/2}^3 p_{3/2}^4 p_{1/2}^0 i_{13/2}^1$
POSITIVE PARITY					
642	700	$13/2^+$	24.13	$h_{9/2}^2 f_{7/2}^0 i_{13/2}^0$	$f_{5/2}^2 p_{3/2}^4 p_{1/2}^0 i_{13/2}^1$
1254	1365	$17/2^+$	28.43	$h_{9/2}^2 f_{7/2}^0 i_{13/2}^0$	$f_{5/2}^2 p_{3/2}^4 p_{1/2}^0 i_{13/2}^1$
1379	1861	$(17/2^+)$	23.95	$h_{9/2}^2 f_{7/2}^0 i_{13/2}^0$	$f_{5/2}^2 p_{3/2}^4 p_{1/2}^0 i_{13/2}^1$
1720	1745	$21/2^+$	23.00	$h_{9/2}^2 f_{7/2}^0 i_{13/2}^0$	$f_{5/2}^2 p_{3/2}^4 p_{1/2}^0 i_{13/2}^1$
1975	1947	$(21/2^+)$	30.87	$h_{9/2}^2 f_{7/2}^0 i_{13/2}^0$	$f_{5/2}^4 p_{3/2}^2 p_{1/2}^0 i_{13/2}^1$
2055	1981	$25/2^+$	32.32	$h_{9/2}^2 f_{7/2}^0 i_{13/2}^0$	$f_{5/2}^2 p_{3/2}^4 p_{1/2}^0 i_{13/2}^1$
2077	2023	$21/2^+$	27.80	$h_{9/2}^2 f_{7/2}^0 i_{13/2}^0$	$f_{5/2}^2 p_{3/2}^4 p_{1/2}^0 i_{13/2}^1$
2404	2347	$25/2^+$	35.75	$h_{9/2}^1 f_{7/2}^0 i_{13/2}^1$	$f_{5/2}^3 p_{3/2}^2 p_{1/2}^0 i_{13/2}^1$

Continued in next page

TABLEII – continued from previous page

Level Energy		$J^\pi$	Probability	Proton	Neutron
EXPT	SM				
2486	2001	23/2 <sup>+</sup>	12.82	$h_{9/2}^0 f_{7/2}^0 i_{13/2}^0$	$f_{5/2}^0 p_{3/2}^0 p_{1/2}^0 i_{13/2}^0$
2500	2337	23/2 <sup>+</sup>	19.05	$h_{9/2}^0 f_{7/2}^0 i_{13/2}^0$	$f_{5/2}^0 p_{3/2}^0 p_{1/2}^0 i_{13/2}^0$
2274	2318	27/2 <sup>+</sup>	22.42	$h_{9/2}^1 f_{7/2}^0 i_{13/2}^1$	$f_{5/2}^1 p_{3/2}^4 p_{1/2}^0 i_{13/2}^{14}$
2523	2375	27/2 <sup>+</sup>	26.22	$h_{9/2}^2 f_{7/2}^0 i_{13/2}^0$	$f_{5/2}^2 p_{3/2}^4 p_{1/2}^0 i_{13/2}^{13}$
2977	2667	27/2 <sup>+</sup>	31.61	$h_{9/2}^2 f_{7/2}^0 i_{13/2}^0$	$f_{5/2}^3 p_{3/2}^3 p_{1/2}^0 i_{13/2}^{13}$
2867	2620	29/2 <sup>+</sup>	35.78	$h_{9/2}^2 f_{7/2}^0 i_{13/2}^0$	$f_{5/2}^2 p_{3/2}^4 p_{1/2}^0 i_{13/2}^{13}$
2863	2758	31/2 <sup>+</sup>	53.28	$h_{9/2}^2 f_{7/2}^0 i_{13/2}^0$	$f_{5/2}^2 p_{3/2}^4 p_{1/2}^0 i_{13/2}^{13}$
3232	2949	31/2 <sup>+</sup>	32.75	$h_{9/2}^2 f_{7/2}^0 i_{13/2}^0$	$f_{5/2}^4 p_{3/2}^2 p_{1/2}^0 i_{13/2}^{13}$
3236	2782	33/2 <sup>+</sup>	52.68	$h_{9/2}^2 f_{7/2}^0 i_{13/2}^0$	$f_{5/2}^2 p_{3/2}^4 p_{1/2}^0 i_{13/2}^{13}$
3242	3185	33/2 <sup>+</sup>	57.96	$h_{9/2}^2 f_{7/2}^0 i_{13/2}^0$	$f_{5/2}^3 p_{3/2}^3 p_{1/2}^0 i_{13/2}^{13}$
3264	3226	33/2 <sup>+</sup>	30.14	$h_{9/2}^2 f_{7/2}^0 i_{13/2}^0$	$f_{5/2}^2 p_{3/2}^4 p_{1/2}^0 i_{13/2}^{13}$
3979	3230	35/2 <sup>+</sup>	51.41	$h_{9/2}^2 f_{7/2}^0 i_{13/2}^0$	$f_{5/2}^2 p_{3/2}^4 p_{1/2}^0 i_{13/2}^{13}$
4146	3517	35/2 <sup>+</sup>	54.27	$h_{9/2}^2 f_{7/2}^0 i_{13/2}^0$	$f_{5/2}^3 p_{3/2}^3 p_{1/2}^0 i_{13/2}^{13}$

The calculated level energies for most of the positive parity states with spin  $< 27/2$  are in excellent overlap, within or around 100-keV, with their experimental values. The yrare 17/2<sup>+</sup> state is an exception for which the calculated and the experimental energies differ by  $\sim 500$ -keV. However, it is noteworthy that the spin-parity assignment of the 1379-keV state as second 17/2<sup>+</sup> was by Fant *et al.* [3] and is tentative. This could not be confirmed in the present study. If the parity assignment of the state is changed, it would be the yrast (and only observed) 17/2<sup>-</sup> level with calculated energy of 1214-keV that is in reasonable overlap with the experimental value. It is noted that, in such a scenario, the 737-keV (17/2<sup>-</sup>  $\rightarrow$  13/2<sup>+</sup>) and 596-keV (21/2<sup>+</sup>  $\rightarrow$  17/2<sup>-</sup>) transitions would be M2 ones and, according to the Weisskopf estimate, would translate into lifetimes of  $\sim$  few ns for the states they de-excite. These lifetimes are much less than the  $\gamma$ - $\gamma$  coincidence window (200 ns) of the experiment and, thus, will not impact the observed intensity of the transitions. The yrast and the yrare 23/2<sup>+</sup> state respectively exhibit differences of  $\sim 500$ -keV and  $\sim 200$ -keV between their theoretical and measured values. While the latter can still be perceived as a reasonable overlap, a deviation of the calculated energy by  $\sim 500$ -keV with respect to the experimental one indicates an aberrant representation of the state in the framework of the shell model calculations. It is also noteworthy that the yrast 23/2<sup>+</sup> state is calculated

to be of substantially mixed configurations, compared to the other states of the nucleus, and the numerically dominant partition is only of 13% probability. As far as the positive parity states of spin  $\gtrsim 29/2$  are concerned, the overlap of experimental and calculated energies is of considerable variance. While they excellently agree for the yrast 31/2<sup>+</sup>, the yrare and the third 33/2<sup>+</sup> levels, within  $\sim 100$ -keV, the difference is  $\sim 250$ -450 keV for the 29/2<sup>+</sup> and the yrast 31/2<sup>+</sup> and 33/2<sup>+</sup>. It is still higher,  $\sim 700$ -keV, for 35/2<sup>+</sup>. Such deviations, at the highest excitations observed in the nucleus, can be ascribed to the limitations of the model calculations in representing the associated multiparticle configurations based on the high-j orbitals (that characterize the relevant model space). Most of the positive parity states have been calculated to be of dominant configuration  $\pi(h_{9/2}^2) \otimes \nu(f_{5/2}^{2-4} p_{3/2}^{2-4} i_{13/2}^{13})$ . The exceptions are the yrare 25/2<sup>+</sup> state, for which the calculated dominant configuration is  $\pi(h_{9/2}^1 i_{13/2}^1) \otimes \nu(f_{5/2}^3 p_{3/2}^2 i_{13/2}^{14})$ , and the yrast 27/2<sup>+</sup> state, for which the most probable configuration is  $\pi(h_{9/2}^1 i_{13/2}^1) \otimes \nu(f_{5/2}^1 p_{3/2}^4 i_{13/2}^{14})$ . It is noteworthy that the calculated and the experimental energies of these states agree within  $\sim 50$ -keV that presumably vindicates the interpretation of their underlying excitations.

If the 2156-keV state is assigned a spin-parity of 25/2<sup>+</sup>, as discussed in the previous section, following an E2 assignment for the 182-keV transition (that de-excites

the level), the level is then the yrare  $25/2^+$  and exhibits a reasonable overlap, within  $\sim 200$  keV, with the calculated energy (2347-keV). The current yrare  $25/2^+$  at 2404-keV is then the third  $25/2^+$  state and its energy is in excellent agreement with the theoretical value of 2383-keV. Once again, since there is no direct experimental evidence to corroborate the spin-parity assignment of the state at 2156-keV, this has not been included in the table.

It may thus be summed up that the observed excitation scheme of the  $^{203}\text{Po}$  nucleus could be satisfactorily interpreted within the framework of the large basis shell model calculations. The specific deviations might have resulted from the limitations of the Hamiltonian that requires further refinements. The latter is expected to be facilitated by the availability of experimental data through endeavors such as the present study.

## V. CONCLUSION

The level structure of the  $^{203}\text{Po}$  nucleus has been probed following its population in  $^{194}\text{Pt}(^{13}\text{C},4n)$  reaction at  $E_{lab} = 74$  MeV. The excitation scheme of the nucleus has been established upto  $\sim 5$  MeV and spin  $\sim 18\hbar$ . Twenty new  $\gamma$ -ray transitions have been added in the level scheme of the the nucleus and spin-parity assignments have been either made or confirmed for a number of states therein. The observed level scheme has been satisfactorily interpreted within the framework of large basis shell model calculations wherein the excited states of the nucleus have been ascribed to proton excitations in  $h_{9/2}$  and  $i_{13/2}$  orbitals outside the  $Z = 82$

closure and neutron excitations in  $f_{5/2}$ ,  $p_{3/2}$  and  $i_{13/2}$  orbitals in the  $N = 126$  shell. The overlap between the experimental and the calculated level energies, of  $^{203}\text{Po}$ , upholds the credibility of the shell model in catering to a microscopic description of the excitation scheme even for heavy nuclei in the  $A \sim 200$  region and in model space consisting of high-j orbitals. Further refinements in the model calculations are envisaged to follow the availability of experimental data.

## Acknowledgments

The authors wish to thank the staff associated with the Pelletron Facility at IUAC, New Delhi, for their help and support during the experiment. We record our deepest gratitude for Late Prof. Asimananda Goswami and Mr. Pradipta Kumar Das, of the Saha Institute of Nuclear Physics (SINP), Kolkata, for their guidance, help and active contribution in the target preparation. Help and support received from Mr. Kausik Basu (UGC-DAE CSR, KC) during the experiment, is appreciated. Help of V. Vishnu Jyothi during the experiment is also acknowledged. P.C.S. acknowledges a research grant from SERB (India), CRG/2019/000556. B.M. acknowledges the support from Department of Science and Technology, Government of India through DST/INSPIRE Fellowship (IF200310). U.G. acknowledges the support from US National Science Foundation through Grant No. PHY1762495. This work is partially supported by the Department of Science and Technology, Government of India (No. IR/S2/PF-03/2003-II).

- 
- [1] V. Rahkonen, B. Fant, C. J. Herrlander, K. Honkanen, A. Källberg, and T. Weckström, Nucl. Phys. A **441**, 11 (1985).
  - [2] T. Weckström, B. Fant, T. Lönnroth, V. Rahkonen, A. Källberg, and C. J. Herrlander, Z. Phys. A **321**, 231 (1985).
  - [3] B. Fant, T. Weckström, V. Rahkonen, C. J. Herrlander, and A. Källberg, Nucl. Phys. A **453**, 77 (1986).
  - [4] S. Muralithar, K. Rani, R. Kumar, R. P. Singh, J. J. Das, J. Gehlot, K. S. Golda, A. Jhingan, N. Madhavan, S. Nath, et al., Nucl. Instr. Meth. Phys. Res. A **622**, 281 (2010).
  - [5] S. Das, S. Samanta, S. Chatterjee, A. Ghosh, R. Bhattacharjee, R. Raut, S. S. Ghugre, and A. K. Sinha, Proc. DAE Symp. Nucl. Phys. **62**, 1066 (2017).
  - [6] R. K. Bhowmik, A. K. Jain, and D. C. Biswas, Proc. DAE Symp. Nucl. Phys. **44B**, 422 (2001).
  - [7] D. C. Radford, Nucl. Instr. Meth. Phys. Res. A **361**, 297 (1995).
  - [8] S. Samanta, S. Das, R. Bhattacharjee, S. Chatterjee, S. S. Ghugre, A. K. Sinha, U. Garg, Neelam, N. Kumar, P. Jones, et al., Phys. Rev. C **97**, 014319 (2018).
  - [9] S. Samanta, S. Das, R. Bhattacharjee, S. Chatterjee, S. S. Ghugre, A. K. Sinha, U. Garg, Neelam, N. Kumar, P. Jones, et al., Phys. Rev. C **99**, 014315 (2019).
  - [10] R. Palit, H. C. Jain, P. K. Joshi, S. Nagaraj, B. V. T. Rao, S. N. Chintalapudi, and S. S. Ghugre, Pramana **54**, 347 (2000).
  - [11] URL [www.nndc.bnl.gov/ensdf/](http://www.nndc.bnl.gov/ensdf/).
  - [12] P. B. Semmes, R. A. Braga, R. W. Fink, J. L. Wood, and J. D. Cole, Nucl. Phys. A **464**, 381 (1987).
  - [13] T. Kibédi, T. W. Burrows, M. B. Trzhaskovskaya, P. M. Davidson, and J. C.W. Nestor, Nucl. Instr. Meth. Phys. Res. A **589**, 202 (2008).
  - [14] B. Fant, T. Weckström, and A. Källberg, Phys. Scr. **41**, 652 (1990).
  - [15] Madhu, K. Yadav, A. Y. Deo, Pragati, P. C. Srivastava, S. K. Tandel, S. G. Wahid, S. Kumar, S. Muralithar, R. P. Singh, et al., Phys. Rev. C **105**, 034307 (2022).
  - [16] K. Yadav, A. Y. Deo, Madhu, Pragati, P. C. Srivastava, S. K. Tandel, S. G. Wahid, S. Kumar, S. Muralithar, R. P. Singh, et al., Phys. Rev. C **105**, 034307 (2022).
  - [17] V. Bothe, S. K. Tandel, S. G. Wahid, P. C. Srivastava, B. Bhoj, P. Chowdhury, R. V. F. Janssens, F. G. Kondev,

- M. P. Carpenter, T. Lauritsen, et al., Phys. Rev. C **105**, 044327 (2022).
- [18] G. H. Herling and T. T. S. Kuo, Nucl. Phys. A **181**, 113 (1972).
- [19] B. A. Brown, MSU NSCL Report p. 1289 (2004).